Hall Thruster Erosion Prediction Using A Hydrodynamic Plasma Model And Sputtering Simulation

IEPC-2007-34

Presented at the 30th International Electric Propulsion Conference, Florence, Italy
September 17-20, 2007

John T. Yim* and Iain D. Boyd†
University of Michigan, Ann Arbor, MI, 48109, USA

and

Michael Keidar‡
George Washington University, Washington, DC, 20052, USA

One of the challenges facing further utilization of Hall thrusters for space missions is establishing valid lifetime predictions. A combination of the use of a hydrodynamic code and a molecular dynamics code is presented for Hall thruster erosion modeling. The hydrodynamic model simulates the plasma flow within the acceleration channel of an SPT-100 thruster to calculate the ion flux to the walls. The molecular dynamics model simulates the sputtering of boron nitride, a common Hall thruster wall material, to calculate sputter yields at low ion impact energies. Results from both models are shown as well as a qualitative comparison of sample erosion profiles with experimental data.

Nomenclature

B	Magnetic field [T]
E	Electric field [V/m]
E_{ion}	Ionization energy [eV]
I_d	Discharge current [A]
Q	Heat (power density) [W/m^3]
T	Temperature [K]
V	Velocity [m/s]
V_d	Discharge voltage [V]
a	Sound speed [m/s]
e	Elementary charge [C]
j	Current density [A/m^2]
k	Boltzmann constant [J/K]
m	Particle mass [kg]
$\dot{m}$	Mass flow rate [mg/s]
n	Number density [m^{-3}]
p	Pressure [N/m^2]
s	Secondary electron emission coefficient
t	Time [s]
β	Ionization rate [m^3/s]

*Graduate Student, Aerospace Engineering, johnyim@umich.edu.
†Professor, Aerospace Engineering, iainboyd@umich.edu.
‡Assistant Professor, Mechanical and Aerospace Engineering, keidar@gwu.edu.

μ	Mobility [$m^2/(V\ s)$]
ν	Collision frequency [s^{-1}]
ρ	Density [kg/m^3]
σ_{en}	Electron-atom collision cross section [m^2]
σ_{ion}	Electron impact ionization cross section [m^2]
ϕ	Potential [V]

Subscript

a	Neutral atom
e	Electron
i	Ion
r	Radial
s	Sheath
z	Axial

I. Introduction

The high specific impulse of Hall thrusters makes them an attractive option for certain classes of space missions due to their reduced propellant mass requirements. However, due to low thrust, the lifetime requirements are higher, particularly for the propulsion system itself. For further acceptance and incorporation into future space missions, the lifetimes of these thrusters need to be validated. However, since these lifetime requirements span into the thousands and tens of thousands of hours, the experimental demonstration of lifetime can be time-consuming as well as expensive. Thus computational modeling and prediction of thruster lifetime is a useful tool for these purposes and has been under recent development.[1–4]

For Hall thrusters, one of the main life-limiting factors is the erosion of the acceleration channel walls. Ions from the discharge plasma gradually erode away the wall material until the softer components of the thruster, such as the magnetic field coils, are exposed and eventually fail. To model this wall erosion, typically the ion flux to the walls is calculated using some method and then angle and energy-dependent sputter yields of the wall material are used to calculate the erosion rates. In this work, we present a hydrodynamic model of the plasma flow within a Hall thruster to find the ion flux to the walls and a molecular dynamics model of low energy xenon ion bombardment of boron nitride to calculate the sputter yields.

An overview of the hydrodynamic and molecular dynamics models is described in the next section. Then, the following section will provide results from the two models and comparisons to experimental data. Results of a sample erosion prediction for the SPT-100 thruster are also presented. Lastly, this is followed by conclusions and areas of future improvement.

II. Methods

One of the eventual goals of this research is to provide a useful tool for erosion and lifetime prediction that can be used in future Hall thruster design and development work. A hydrodynamic model of the plasma flow within a Hall thruster offers fairly quick turnaround times for results while maintaining some robustness across different types of thrusters under various operating conditions. It offers some balance between semi-empirical models and particle-based methods and can be used in conjunction with these other models as well as experimental results to obtain a more comprehensive analysis of channel wall erosion. The hydrodynamic method presented here models the ions, neutral atoms, and electrons as separate fluids and solves the associated equations on an axisymmetric mesh of the channel region. The ion fluxes to the walls are calculated using this method.

The sputter yields used in erosion simulations are typically curve fits applied to existing experimental data. However, experimental data is sparse, especially for very low energy ion impacts. Until very recently, experimental data below 300 eV did not exist. Depending on the assumed threshold energy and the method of curve fit extrapolation of the sputter yield into the low energy regime, the resulting erosion rates can vary significantly.[5] Therefore, a molecular dynamics (MD) method is used to calculate the sputter yields of boron nitride under very low energy xenon ion impacts. The MD method has been used before to simulate sputtering processes for other systems.[6,7] An alternative to MD methods are Monte Carlo (MC) methods,

which are also used for sputtering analyses.[8–11] These methods are less computationally intensive than the MD methods. At very low energies, however, some of the assumptions that these MC methods are based on, such as binary collisions, do not necessarily hold. The sputter yield results from MC methods can also be sensitive to certain input parameters such as the surface binding energy, which are sometimes uncertain.[12] Thus, the MD method is chosen here for very low energy sputter analyses.

A. Hydrodynamic Method

A hydrodynamic description of the quasi-neutral plasma flow within the thruster is used.[5,13] The ions–only singly charged ions are considered for this model–are modeled using a finite-volume flux-splitting method on an axisymmetric Cartesian mesh.[14] The governing ion equations can be written in conservative form as

$$\frac{\partial \rho}{\partial t} + \frac{\partial \left(\rho V_z\right)}{\partial z} + \frac{\partial \left(\rho V_r\right)}{\partial r} = \beta n_a \rho \tag{1}$$

$$\frac{\partial \left(\rho V_z\right)}{\partial t} + \frac{\partial \left(\rho a^2 + \rho V_z^2\right)}{\partial z} + \frac{\partial \left(\rho V_z V_r\right)}{\partial r} = enE_z + \beta n_a V_a \rho \tag{2}$$

$$\frac{\partial \left(\rho V_r\right)}{\partial t} + \frac{\partial \left(\rho V_z V_r\right)}{\partial z} + \frac{\partial \left(\rho a^2 + \rho V_r^2\right)}{\partial r} = enE_r \tag{3}$$

The ions are assumed to be unmagnetized since the Larmor radius is much larger than the length of the channel. The ions are also assumed to be cold, eliminating the need for the ion energy equation as well as the pressure term in the momentum equations. The source terms on the right hand side of the above equations result from the effects of ionization and the electric field. The ionization rate is found from[15]

$$\beta = \sigma_{\text{ion}} V_{th} \left(1 + 2\frac{kT_e}{eE_{\text{ion}}}\right) \exp\left(-\frac{eE_{\text{ion}}}{kT_e}\right) \tag{4}$$

where V_{th} is the electron thermal velocity. The ionization cross section is dependent on electron energy,[16] but for simplicity it is approximated here as a constant.

The components of the electric field are calculated from the potential field. If the electrons are assumed to be mainly constrained and in thermal equilibrium along the magnetic field lines, the concept of a thermalized potential can be used to calculate the potential field within the thruster through

$$\phi = \phi^* + \frac{kT_e}{e} \log\left(\frac{n}{n^*}\right) \tag{5}$$

where the starred terms are reference values. In this case, the channel centerline values are chosen to be the reference. A prescribed centerline electron temperature, based off of the centerline radial magnetic field profile, is shown in Fig. 1 along with the rest of the electron temperature field ranging from the anode to the thruster exit. The contours of Fig. 1 follow the magnetic field lines as per the assumptions of the thermalized potential. The magnetic field data available for use for this work was initially on a rather coarse mesh, so a simple interpolation scheme is used. Contour lines of the radial component of the magnetic field are shown in Fig. 2.

For the neutral atoms, a one-dimensional flow is considered. The density of the neutrals is also governed by a continuity equation similar to Eq. (1) except the source term is negative since ionization depletes the neutrals. An axial momentum equation is used to calculate the velocity of the neutral atoms.

Since several of the assumptions of the governing equations, such as quasi-neutrality, break down within the sheath, the lateral boundaries of the simulation are set at the plasma-sheath interface and not the actual wall boundaries. At the sheath edge, a calculated relation between the ion velocity and the electric field is used to set the density gradient through[17,18]

$$\nabla n = -\frac{kT_e}{enE} \tag{6}$$

The potential drop across the sheath also depends on the ion velocity entering the sheath and the secondary electron emission.[19]

$$\phi_{\text{s}} = \frac{kT_e}{e} \ln\left(\frac{1-s}{V_{\text{s}}\sqrt{2\pi m_e/(kT_e)}}\right) \tag{7}$$

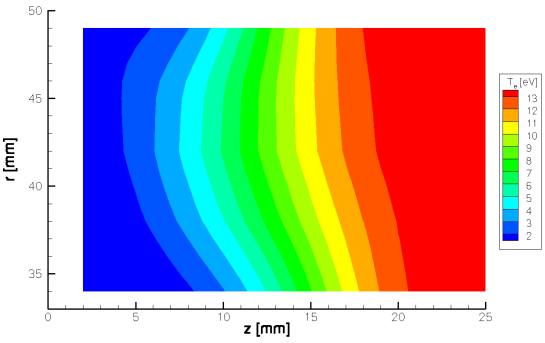

Figure 1. The electron temperature field.

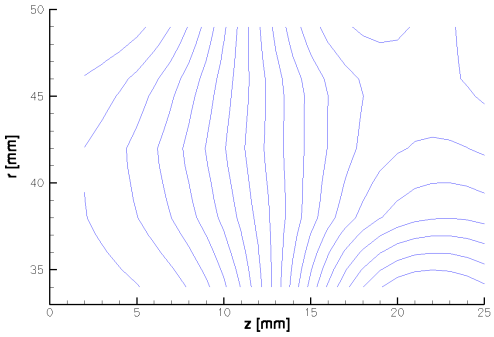

Figure 2. Contour lines of the radial component of the magnetic field.

The secondary electron emission coefficient is modeled after experimental observations.[20]

$$s = 0.54 + \frac{1 - 0.54}{40} \frac{kT_e}{e} \tag{8}$$

For the governing ion equations, Eqs. (1)-(3), a Roe solver is used to calculate the fluxes across each of the cell interfaces, which in turn are used to update the cell values at each time step.[21] The mesh consists of 25×30 square cells 1.0 mm on a side. The simulation is iterated until it converges to a representative state. The simulation is run for an SPT-100 thruster operating with a discharge voltage of 300 V, discharge current of 4.5 A, and a mass flow rate of 5.0 mg/s.

B. Molecular Dynamics Method

The molecular dynamics method solves Newton's law of motion for a system of particles, which in this case are atoms. The interactions among the particles are determined through interatomic potential functions which depend on particle positions only. Since only conservative forces are considered, the negative gradient of the potential function provides the forces on each particle arising from the particles around it. The forces are used to calculate the particle velocities, which in turn are used to calculate the particle positions using the traditional leapfrog method. Averaging over a sufficient number of timesteps and events, the macroscopic quantities of interest, here specifically, the sputter yield of boron nitride from impacting xenon ions, can be obtained.

For the interactions of the boron and nitrogen atoms with one another, the interatomic potential presented by Albe *et al.* is used.[22,23] This is a modified form of the bond-order potential first proposed by Tersoff for multi-component systems.[24] The Tersoff potential has been used to model other covalent systems successfully and the general form is well suited for the purposes here. In particular, Albe *et al.* have used their potential to model hexagonal boron nitride, which is the same form that is modeled here.[22] They achieve good agreement with values of structural and elastic properties, such as the bulk modulus and lattice constant, recorded from other methods including experimental data. Bond-order potentials, in general, are better suited than most other conventional potential functions to describe bond interactions based on different bonding environments, such as the number and type of other bonds involved, rather than being optimized for a particular lattice structure.[25]

The potential is of the form

$$\Phi = \frac{1}{2} \sum_{i \neq j} f_c\left(r_{ij}\right) \left[f_R\left(r_{ij}\right) - b_{ij} f_A\left(r_{ij}\right) \right] \tag{9}$$

where f_c is a cutoff function limiting the range of the potential. The f_R and f_A terms are the repulsive and attractive parts of the potential, respectively. The b_{ij} term is a modifier to the attractive force component that takes into account third-body bond stretching and bending, and r_{ij} is the distance from particle i to particle j. The potential is dependent on particle positions only.

The repulsive and attractive components of this potential are similar in form and are based on a Morse potential[26]

$$f_R\left(r_{ij}\right) = \frac{D_0}{S-1}\exp\left[-\beta\sqrt{2S}(r_{ij}-r_0)\right] \tag{10}$$

$$f_A\left(r_{ij}\right) = \frac{SD_0}{S-1}\exp\left[-\beta\sqrt{\frac{2}{S}}(r_{ij}-r_0)\right] \tag{11}$$

where D_0 is the dimer energy and r_0 is the dimer separation. S and β are fitting constants.

The flexibility of bond-order potentials stems from the modifier term b_{ij}, which for this potential is given as

$$b_{ij} = \left(1+\gamma^n\chi^n\right)^{-1/2n} \tag{12}$$

$$\chi = \sum_{k\neq i,j} f_c(r_{ik})g(\theta_{ijk})h(r_{ij},r_{ik}) \tag{13}$$

$$g(\theta_{ijk}) = 1 + \frac{c^2}{d^2} - \frac{c^2}{d^2+(m-\cos(\theta_{ijk})^2} \tag{14}$$

$$h(r_{ij},r_{ik}) = \exp\left[\lambda^3(r_{ij}-r_{ik})^3\right] \tag{15}$$

where the k index indicates the third particle under consideration (θ_{ijk} would be the angle between ij and ik) and γ, n, c, d, m, and λ are all constants.

The cutoff function, f_c, used in this work is[27]

$$f_c\left(r_{ij}\right) = \begin{cases} 1, & r_{ij} \leq R-D \\ \exp\left(\alpha\frac{x^3}{x^3-1}\right), & R-D < r_{ij} < R+D \\ 0, & r_{ij} \geq R+D \end{cases} \tag{16}$$

$$x = \frac{r_{ij}-(R-D)}{2D} \tag{17}$$

where $\alpha = 3$ minimizes the magnitude of the local extremum of the first derivative. This function transitions smoothly from unity, at the inner boundary, to zero, at the outer boundary, while both the first and second derivatives are zero at both ends.

A modification is made to the potential function. Initial runs using the Albe potential did not conserve energy successfully. This stemmed from the g component within the modifier b_{ij}, as seen in Eqs. (12) and (13), for boron-boron interactions. The coefficients c and d are adjusted from 0.52629 and 0.001587 to 3.316257 and 0.01 respectively, since the low value of d makes the third term in Eq. (14) very sensitive to the angle θ_{ijk}. This is shown in Fig. 3. As can be seen, the original coefficients create a very steep profile that would require a much smaller timestep to traverse smoothly. The value c is also altered to keep the second term of g given in Eq. (14) the same value as it was originally. Table 1 lists the constants used for this potential and their values depending on the identity of the pair i and j.

For the interactions involving the xenon ions, a Molière potential is used. The Molière potential is a purely repulsive potential. Since the van der Waals attraction of the xenon with the boron and nitrogen atoms is much weaker than the covalent attraction the boron nitride has within itself, a purely repulsive force is acceptable.[28] This potential is based on a screened Coulomb repulsion and has the form

$$\Phi = \frac{Z_iZ_je^2}{4\pi\epsilon_0 r_{ij}}\left[0.35\exp\left(-0.3\frac{r_{ij}}{a_F}\right) + 0.55\exp\left(-1.2\frac{r_{ij}}{a_F}\right) + 0.10\exp\left(-6.0\frac{r_{ij}}{a_F}\right)\right] \tag{18}$$

where a_F is the Firsov screening length.

The boron nitride considered here is in hexagonal form, similar in structure to that of graphite. The domain consists of 32 sheets of 12 × 24 hexagons, or 38400 particles arranged in a 10.4 nm × 10.4 nm × 3.0 nm box. A smaller domain of 24 sheets of 10 × 18 hexagons, or 18144 particles in a 7.8 nm × 7.8 nm × 2.5 nm box is used for ion energies below 150 eV since it reduces the computational time with no significant effect on the results for those cases. Periodic boundary conditions are applied in the lateral directions. The bottom layer of atoms is kept immobile to keep the structure as a whole from translating due to ion impacts. The next two layers directly above the bottom immobile layer are designated as a thermostatted region.

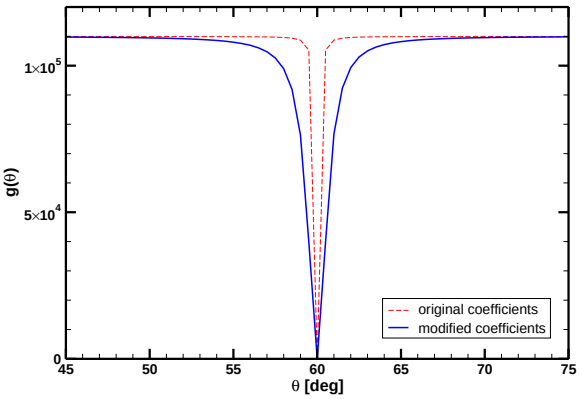

Figure 3. The g term in Eq. (14) for B-B bonds using the original and modified coefficients.

	B-B	N-N	B-N
R [Å]	2.0	2.0	2.0
D [Å]	0.1	0.1	0.1
D_0 [eV]	3.08	9.91	6.36
r_0 [Å]	1.59	1.11	1.33
β [Å^{-1}]	1.5244506	1.92787	2.043057
S	1.0769	1.0769	1.0769
n	3.9929061	0.6184432	0.364153367
γ	0.0000016	0.019251	0.000011134
λ [Å^{-1}]	0.0	0.0	1.9925
c	3.316257	17.7959	1092.9287
d	0.01	5.9484	12.38
m	0.5	0.0	-0.5413

Table 1. Coefficient values used for the boron nitride potential function.

The two thermostatted layers are regulated using a Berendsen thermostat which rescales the velocities of the particles involved.[28,29] The temperature of the rest of the boron nitride is regulated through conduction. The boron nitride is initialized and regulated at a temperature of 150°C, which is approximately the temperature of boron nitride samples in experimental sputtering studies.[30,31] This temperature is set through the initial velocities, which are randomized in such a way as to remove any bulk motion. Since the instantaneous temperature of the block incurs large statistical scatter, a method to evaluate the average temperature of the block is needed. A sub-relaxation technique is used to monitor the macroscopic temperature of the BN system.[32]

After the boron nitride surface equilibrates, a xenon ion is injected far above the surface with a specified energy. The angle incident to the surface normal is set to 45 degrees, where experimental data exist from different studies. The other angular component is randomized to minimize the effects of lattice orientation in the lateral directions. In addition, the upper regions of boron nitride form an amorphous layer that contains no observable orientation for the structure after a sufficient number of ion impact events. After each ion impact, the boron nitride system is re-equilibrated to the proper temperature before proceeding with the next ion impact.

In order to speed up the calculations, several computational techniques are employed. Neighbor lists, both Verlet neighbor and linked cell lists, are used so that each possible particle pair did not need to be evaluated at each timestep.[33] Especially for a short range potential, such as the modified Tersoff described above, this removes the need to perform O(N^2) calculations for every timestep. The simulation code is also parallelized with OpenMP directives for use on multi-processor machines. A timestep of 0.1 fs is used to run the simulation.

The simulation is first run for a number of ion impacts until a representative form of boron nitride is formed with the amorphous layers near the surface. This state is then used as the initial block to test a sufficient number of individual ion impact events. The ion initial positions and velocities are randomized, but the energy and incident angle are kept the same. From these impact events, the statistics are gathered and analyzed to calculate the sputter yields. The properties of the ejected atoms are also kept track of to produce differential sputtering data. The ion energies examined varies from 350 eV, in order to compare to experimental data, to 50 eV, which is near where the sputter threshold energy for this system is expected to lie.

In a previous report, the sputter yields calculated with this method were much higher than expected.[34] This has been corrected for, in part, with use of a larger domain and better temperature regulation. With periodic boundaries, the energy of an impacting ion might cross over back into the simulation domain and artificially increase the energy of the region, thus leading towards a greater possibility of ejected atoms. Damped periodic boundary conditions may alleviate this problem, but due to the random ion injection location, the periodic boundaries are kept undamped so as to not affect particle trajectories if the ions

happen to impact near a boundary. The temperature of the atoms near the surface were also observed to be much higher than the bulk reading. Thus, proper monitoring of the temperature of the atoms nearest to the surface is used to ensure the temperature is near the desired value before every ion injection into the system.

A quantum-statistical approach presented by Wilhelm is also used for comparison of the sputter yields at very low energies.[35] With this approach, a three-body interaction of the ion and two atoms of a polycrystalline solid is considered and the probabilities of the ion scattering versus an atom sputtering are used to calculate the rate of sputter. Wilhelm's approximation for the sputter yield at energies between the threshold energy and about 100 eV is given by

$$S(E) \approx \frac{1}{24} h_{2/1} \sigma(E_0) N^{2/3} \left(\frac{(M/m)^2}{1 + 2M/m} \right)^{3/2} \frac{(E - E_0)^2}{E_0^2} \tag{19}$$

where S is the sputter yield, E and E_0 are the ion energy and threshold energy respectively, $h_{2/1}$ is a dimensionless coefficient dependent on the perturbation operator of the Hamiltonian of the system between the initial and final states and their corresponding volumes, σ is the total scattering cross section, N is the number density of the atoms in the solid, and m and M are the mass of the ion and the target atom respectively. Since not all of the parameters required for Eq. (19) are known, only a qualitative form of the equation is used in this work for comparative purposes. Equation (19) is proportional to

$$S(E) \approx a(E - E_0)^2 \tag{20}$$

where a is a fitting coefficient.

III. Results and Discussion

The hydrodynamic model is used to simulate the plasma flow field within an SPT-100 thruster discharge channel. Figures 4 and 5 show sample results of the plasma density and potential, respectively. For erosion analysis studies, the main focus of the hydrodynamic model is to provide the energies, angles, and flux of the impacting ions along the channel walls. The ions accelerate as they travel to the walls through the sheath potential drop given in Eq. 7. The sheath potential along the wall length is shown in Fig. 6. The ion flux, in the form of current density, to the walls can then be found and is plotted in Fig. 7.

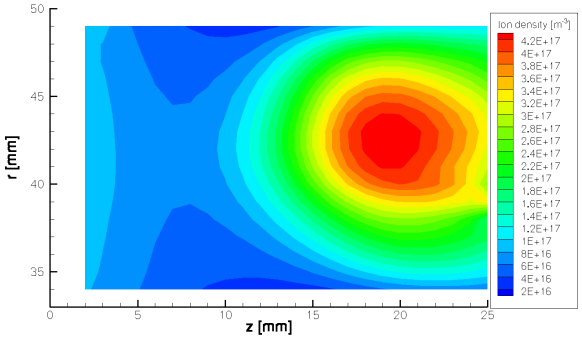

Figure 4. The plasma density.

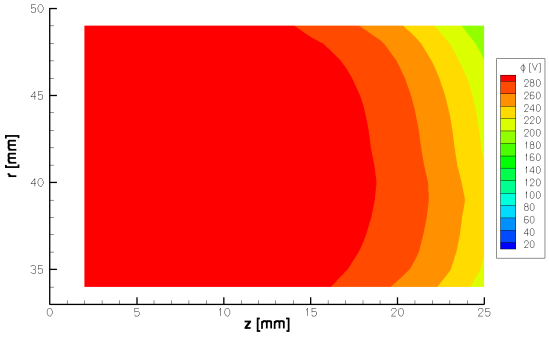

Figure 5. The plasma potential.

The calculated sputter yields of hexagonal boron nitride are compared to experimental results for ions incident at 45 degrees at various energies in Fig. 8. For the MD results, at least 100 ion impacts are simulated for each energy. The experimental results are obtained from different methods including weight loss, quartz crystal microbalance (QCM) measurements, and laser profilometry.[30,31,36,37] For the simulation results and the results from Yalin *et al.*, the density of HBC grade BN, 1.98 g/cm^3, is used to present the results.[36] The grades of boron nitride for the results from Garnier *et al.* and Britton *et al.* are unknown. It should also be noted that the data from Britton *et al.* is at an incidence angle of 40 degrees as they did not present any results at 45 degrees. The QCM method can only measure particles that condense on the QCM. The lower limit shown in Fig. 8 corresponds to the actual readings of the QCM measurements while the upper limit

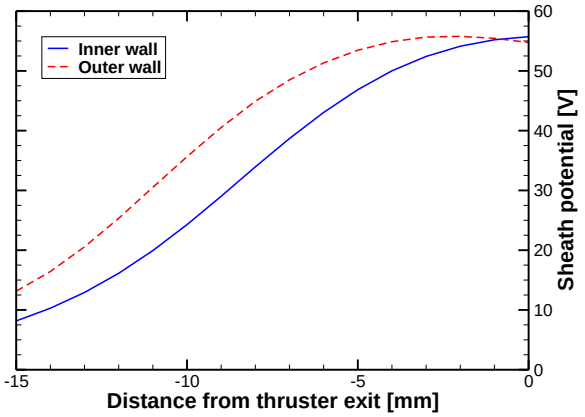

Figure 6. The sheath potential.

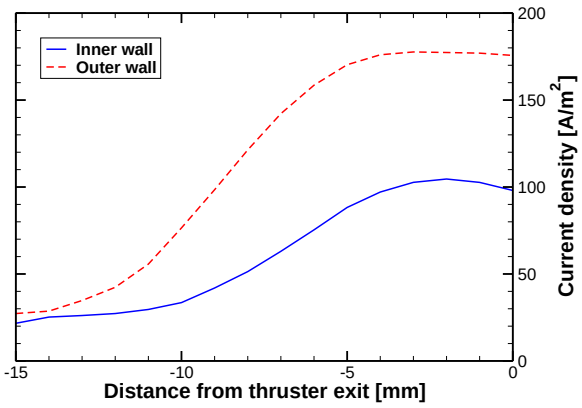

Figure 7. The ion current density to the walls.

shown is an approximation of the total sputter yield if the non-condensible components, specifically nitrogen, are estimated to be in equal stoichiometry to the condensed products, boron and boron compounds.

The simulation results for ion energies less than 150 eV agree with experimental trends and fall within the expected value range. The simulation data at 250 eV and 350 eV, however are higher than any of the experimental data presented in that energy range. One possible reason behind these higher sputter yields may be from the fact that in the simulation, a greater proportion of nitrogen is sputtered as compared to boron. Nitrogen is sputtered about twice as much as boron in the 350 eV case, and at 50 eV, only nitrogen is observed to sputter. In particular, the nitrogen is often sputtered as N_2 molecules. The nitrogen-nitrogen interaction saturates their bonding and makes it difficult for other bonds to form with the pair, and thus they escape the boron nitride block more easily. This BN potential in particular has been shown to have reliable accuracy for B_nN_m clusters, especially for $n, m \leq 3$, in addition to various bulk BN structures.[22] However, an electron spectroscopy for chemical analysis (ESCA) study performed on a boron nitride sample after sputtering shows little variation between the boron and nitrogen ratios on the surface before and after sputtering.[30] This would seem to indicate that they sputter in roughly equal proportions, at least from the surface level.

Quantum-statistical analysis of low energy sputtering is also used to provide a curve fit near the threshold energy. In general, the sputter yield at very low energies is predicted to be proportional to the square of the energy above the threshold value as seen in Eq. (20). The curve fit is based on this relation and is matched to the data points below 150 eV. Then, the corresponding threshold energy, E_0, is approximately 14 eV while $a = 3.98 \times 10^{-6}$ for sputter yields measured in mm^3/C. Figure 9 shows this fit of the quantum-statistical trend with the results of the model. The threshold energy calculated from this method is lower than prior estimates. Possible causes may be from the assumptions made in the quantum-statistical analysis. The analysis is originally performed for polycrystalline monatomic metals as opposed to graphite-like sheets of a binary compound.

The calculated sputter yield is used in conjunction with the calculated ion current density to the thruster channel walls to determine the beginning-of-life (BOL) erosion rates. Since the erosion rate of the walls over time has been observed to decrease over time, particularly early in the lifetime, the BOL erosion rates can not be directly used to calculate erosion profiles at a later time. However, for comparative purposes, the profiles of the initial erosion rates along the walls are multiplied by the same proportion to be comparable to the values of erosion measured after 160 hours of operation.[38] As seen in Fig. 10, the outer wall erosion is overestimated, though the shape of the profile is matched fairly well. The inner wall has lower erosion rates than the outer wall and at least qualitatively, again, the shape matches fairly well. The upstream location where erosion begins is overestimated for both walls. This is likely due to the low estimated threshold energy.

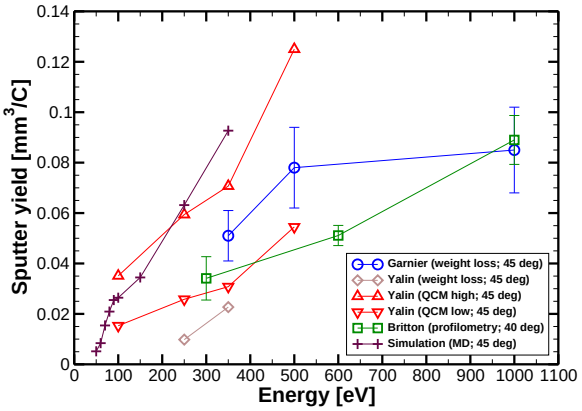

Figure 8. The BN sputter yield results from experiments and simulation for 45° incident ions at various energies.

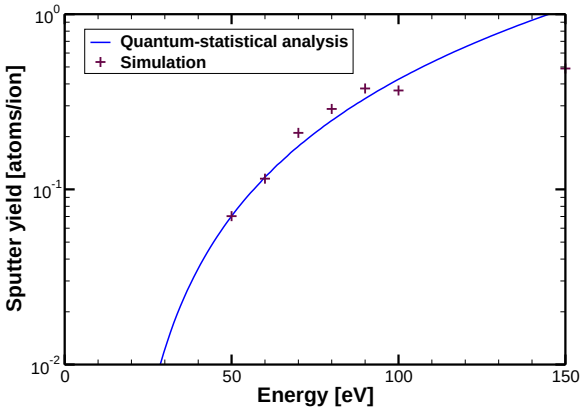

Figure 9. A quantum-statistical analysis fit to the results of the MD simulations.

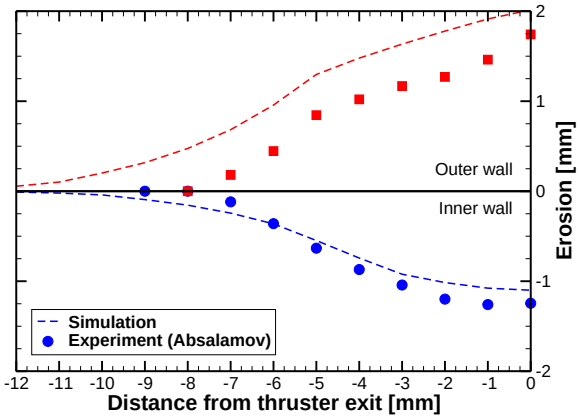

Figure 10. A qualitative comparison of the calculated beginning-of-life erosion rate profiles with the measured erosion profiles after 160 hours.

IV. Conclusion

The future development of erosion analysis tools for Hall thruster design and development requires further refinement of the simulation of ion flux to the walls as well as more accuracy in the calculation of the sputter yields. The hydrodynamic model presented here is one of several options to calculate the ion flux to the walls; it offers quick calculation times, on the order of minutes, while not being as dependent on experimental data as semi-empirical models. The molecular dynamics simulations are computationally expensive, but sputter yields only need to be calculated once. The sputter yields of hexagonal boron nitride at energies below 150 eV follow experimental trends while the calculated sputter yields at 250 eV and 350 eV are higher than expected. A larger proportion of sputtered nitrogen, particularly as N_2, compared to sputtered boron is also observed.

Next steps for the hydrodynamic code include using it to calculate the ion flux to the walls as they erode away. Determining the erosion profiles at various times as well as the erosion rate as a function of time are important steps towards improving Hall thruster lifetime prediction. Further validation against other codes and models as well as measured data for other thrusters and operating conditions is also needed.

Acknowledgments

We would like to thank NASA Glenn Research Center for their support of this work through Grant NNCO4GA56G. John T. Yim would also like to thank the National Science Foundation for their support through their Graduate Research Fellowship Program.

References

[1]Yu, D., Li, Y., and Song, S., "Ion Sputtering Erosion of Channel Wall Corners in Hall Thrusters," *Journal of Physics D: Applied Physics*, Vol. 39, 2006, pp. 2205–2211.

[2]Sommier, E., Allis, M. K., Gascon, N., and Cappelli, M. A., "Wall Erosion in 2D Hall Thruster Simulations," *42nd AIAA/SAE/ASME/ASEE Joint Propulsion Conference and Exhibit*, July 2006, AIAA-2006-4656.

[3]Lovtsov, A., Shagayda, A., and Gorshkov, O., "Semi-Empirical Method of Hall Thrusters Lifetime Prediction," *42nd AIAA/ASME/SAE/ASEE Joint Propulsion Conference and Exhibit*, July 2006, AIAA-2006-4661.

[4]Hofer, R. R., Katz, I., Mikellides, I. G., and Gamero-Castaño, M., "Heavy Particle Velocity and Electron Mobility Modeling in Hybrid-PIC Hall Thruster Simulations," *42nd AIAA/SAE/ASME/ASEE Joint Propulsion Conference and Exhibit*, July 2006, AIAA-2006-4658.

[5]Yim, J. T., Keidar, M., and Boyd, I. D., "An Investigation of Factors Involved in Hall Thruster Wall Erosion Modeling," *42nd AIAA/SAE/ASME/ASEE Joint Propulsion Conference and Exhibit*, July 2006, AIAA 2006-4657.

[6]Zhou, X. W., Wadley, H. N. G., and Sainathan, S., "Low Energy Sputtering of Nickel by Normally Incident Xenon Ions," *Nuclear Instruments and Methods in Physics Research B*, Vol. 234, 2005, pp. 441–457.

[7]Kress, J. D., Hanson, D. E., Voter, A. F., Liu, C. L., Liu, X.-Y., and Coronell, D. G., "Molecular Dynamics Simulation of Cu and Ar Ion Sputtering of Cu (111) surfaces," *Journal of Vacuum Science and Technology A*, Vol. 17, No. 5, 1999, pp. 2819–2825.

[8]Pugacheva, T. S., Jurabekova, F. G., and Valiev, S. K., "Effects of Cascade Mixing, Sputtering and Diffusion by High Dose Light Ion Irradiation of Boron Nitride," *Nuclear Instruments and Methods in Physics Research B*, Vol. 141, 1998, pp. 99–104.

[9]Chen, M., Rohrbach, G., Neuffer, A., Barth, K.-L., and Lunk, A., "Simulation of Boron Nitride Sputtering Process and Its Comparison with Experimental Data," *IEEE Transactions on Plasma Science*, Vol. 26, No. 6, Dec. 1998, pp. 1713–1717.

[10]Greene, J. P., Nemanich, J., Thomas, G. E., and Schiel, S. L., "Noble Gas Sputtering Calculations Using TRIM," *Nuclear Instruments and Methods in Physics Research A*, Vol. 397, 1997, pp. 91–98.

[11]Eckstein, W. and Biersack, J. P., "Computer Simulation of Two-Component Target Sputtering," *Applied Physics A*, Vol. 37, 1985, pp. 95–108.

[12]Urbassek, H. M., "Molecular-Dynamics Simulation of Sputtering," *Nuclear Instruments and Methods in Physics Research B*, Vol. 122, 1997, pp. 427–441.

[13]Yim, J. T., Keidar, M., and Boyd, I. D., "A Hydrodynamic-Based Erosion Model for Hall Thrusters," *29th International Electric Propulsion Conference*, Oct. 2005, IEPC-2005-013.

[14]LeVeque, R. J., "Wave Propagation Algorithms for Hyperbolic Systems," *Journal of Computational Physics*, Vol. 131, No. 2, 1997, pp. 327–353.

[15]Ahedo, E., Martinez, P., and Martinez-Sanchez, M., "Steady and Linearly-Unsteady Analysis of a Hall Thruster with an Internal Sonic Point," *36th AIAA/SAE/ASME/ASEE Joint Propulsion Conference and Exhibit*, July 2000, AIAA 2000-3655.

[16]Sorokin, A. A., Shmaenok, L. A., Bobachev, S. V., Möbus, B., Richter, M., and Ulm, G., "Measurements of Electron-Impact Ionization Cross Sections of Argon, Krypton, and Xenon by Comparison with Photoionization," *Physical Review A*, Vol. 61, 2000, pp. 022723.

[17]Keidar, M., Boyd, I. D., and Beilis, I. I., "Plasma Flow and Plasma-Wall Transition in Hall Thruster Channel," *Physics of Plasmas*, Vol. 8, No. 12, Dec. 2001, pp. 5315–5322.

[18]Godyak, V. A., "Modified Bohm Criterion for a Collisional Plasma," *Physics Letters*, Vol. 89, No. 2, April 1982, pp. 80–81.

[19]Hobbs, G. D. and Wesson, J. A., "Heat Flow Through a Langmuir Sheath in the Presence of Electron Emission," *Plasma Physics*, Vol. 9, 1967, pp. 85–87.

[20]Dunaevsky, A., Raitses, Y., and Fisch, N. J., "Secondary Electron Emission from Dielectric Materials of a Hall Thruster with Segmented Electrodes," *Physics of Plasmas*, Vol. 10, No. 6, June 2003, pp. 2574–2577.

[21]Roe, P. L., "Approximate Riemann Solvers, Parameter Vectors, and Difference Schemes," *Journal of Computational Physics*, Vol. 135, No. 2, 1997, pp. 250–258.

[22]Albe, K., Möller, W., and Heinig, K.-H., "Computer Simulation and Boron Nitride," *Radiation Effects and Defects in Solids*, Vol. 141, 1997, pp. 85–97.

[23]Albe, K. and Möller, W., "Modelling of Boron Nitride: Atomic Scale Simulations on Thin Film Growth," *Computational Materials Science*, Vol. 10, 1998, pp. 111–115.

[24]Tersoff, J., "New Empirical Approach for the Structure and Energy of Covalent Systems," *Physical Review B*, Vol. 37, No. 12, April 1988, pp. 6991–7000.

[25]Leach, A. R., *Molecular modelling : principles and applications*, Prentice Hall, 2001.

[26]Brenner, D. W., "Empirical Potential for Hydrocarbons for Use in Simulating the Chemical Vapor Deposition of Diamond Films," *Physical Review B*, Vol. 42, No. 15, Nov. 1990, pp. 9458–9471.

[27]Los, J. H. and Fasolino, A., "Intrinsic Long-Range Bond-Order Potential for Carbon: Performance in Monte Carlo Simulations of Graphitization," *Physical Review B*, Vol. 68, 2003, pp. 024107.

[28]Kalyanasundaram, N., Moore, M. C., Freund, J. B., and Johnson, H. T., "Stress Evolution Due to Medium-Energy Ion Bombardment of Silicon," *Acta Materialia*, Vol. 54, 2006, pp. 483–491.

[29]Berendsen, H. J. C., Postma, J. P. M., van Gunsteren, W. F., DiNola, A., and Haak, J. R., "Molecular Dynamics with Coupling to an External Bath," *Journal of Chemical Physics*, Vol. 81, No. 8, Oct. 1984, pp. 3684–3690.

[30]Garnier, Y., Viel, V., Roussel, J.-F., and Bernard, J., "Low-Energy Xenon Ion Sputtering of Ceramics Investigated for Stationary Plasma Thrusters," *Journal of Vacuum Science and Technology A*, Vol. 17, No. 6, Nov/Dec 1999, pp. 3246–3254.

[31]Yalin, A. P., Surla, V., Farnell, C., Butweiller, M., and Williams, J. D., "Sputtering Studies of Multi-Component Materials by Weight Loss and Cavity Ring-Down Spectroscopy," *42nd AIAA/SAE/ASME/ASEE Joint Propulsion Conference and Exhibit*, July 2006, AIAA 2006-4338.

[32]Sun, Q. and Boyd, I. D., "Evaluation of Macroscopic Properties in the Direct Simulation Monte Carlo Method," *Journal of Thermophysics and Heat Transfer*, Vol. 19, No. 3, 2005, pp. 329–335.

[33]Haile, J. M., *Molecular Dynamics Simulation : Elementary Methods*, Wiley, 1992.

[34]Yim, J. T., Falk, M., Keidar, M., and Boyd, I. D., "Calculation of Boron Nitride Sputter Yields Under Low Energy Xenon Ion Bombardment," *43rd AIAA/SAE/ASME/ASEE Joint Propulsion Conference and Exhibit*, July 2007, AIAA 2007-5313.

[35]Wilhelm, H. E., "Quantum-Statistical Analysis of Low Energy Sputtering," *Australian Journal of Physics*, Vol. 38, 1985, pp. 125–133.

[36]Yalin, A. P., Rubin, B., Domingue, S. R., Glueckert, Z., and Williams, J. D., "Differential Sputter Yields of Boron Nitride, Quartz, and Kapton Due to Low Energy Xe+ Bombardment," *43rd AIAA/SAE/ASME/ASEE Joint Propulsion Conference and Exhibit*, July 2007, AIAA 2007-5314.

[37]Britton, M., Waters, D., Messer, R., Sechkar, E., and Banks, B., "Sputtering Erosion Measurement on Boron Nitride as a Hall Thruster Material," Tech. rep., NASA, 2002, NASA TM-2002-211837.

[38]Absalamov, S. K. et al., "Measurement of Plasma Parameters in the Stationary Plasma Thruster (SPT-100) Plume and Its Effect on Spacecraft Components," *28th AIAA/SAE/ASME/ASEE Joint Propulsion Conference and Exhibit*, July 1992, AIAA 92-3156.